INTERNATIONAL JOURNAL FOR NUMERICAL METHODS IN FLUIDS
Int. J. Numer. Meth. Fluids 2009; **60**:263–274
Published online 11 August 2008 in Wiley InterScience (www.interscience.wiley.com). DOI: 10.1002/fld.1886

Simulating turbulent Dean flow in Cartesian coordinates

George K. El Khoury[1,*,†], Helge I. Andersson[2] and Bjørnar Pettersen[1]

[1]*Department of Marine Technology, The Norwegian University of Science and Technology, N-7491 Trondheim, Norway*
[2]*Department of Energy and Process Engineering, The Norwegian University of Science and Technology, N-7491 Trondheim, Norway*

SUMMARY

A simplified approach to simulate turbulent flows in curved channels is proposed. A set of governing equations of motion in Cartesian coordinates is derived from the full Navier–Stokes equations in cylindrical coordinates. Terms to first order in the dimensionless curvature parameter are retained, whereas higher-order terms are neglected. The curvature terms are implemented in a conventional Navier–Stokes code using Cartesian coordinates. Direct numerical simulations (DNS) of turbulent flow in weakly curved channels are performed. The pronounced asymmetries in the mean flow and the turbulence statistics observed in earlier DNS studies are faithfully reproduced by the present simplified Navier–Stokes model. It is particularly rewarding that also distinct pairs of counter-rotating streamwise-oriented vortices are embedded in the simulated flow field. Copyright © 2008 John Wiley & Sons, Ltd.

Received 27 February 2008; Revised 16 June 2008; Accepted 16 June 2008

KEY WORDS: channel flow; streamline curvature; roll cells; DNS

1. INTRODUCTION

Turbulent flows along convex or concave surfaces are frequently occurring in a variety of industrial applications. The presence of a centrifugal force due to the inevitable streamline curvature affects not only the mean flow but also the individual components of the Reynolds stress tensor. Typical prototypes of wall-bounded flows with streamline curvature are Görtler flow along a concave surface, Taylor–Couette flow between independently rotating cylinders, and Dean flow in a curved

*Correspondence to: George K. El Khoury, Department of Marine Technology, The Norwegian University of Science and Technology, N-7491 Trondheim, Norway.
†E-mail: george.e.khoury@ntnu.no

Contract/grant sponsor: The Research Council of Norway
Contract/grant sponsor: NTNU

channel. A common feature of these flows is that a centrifugal instability may give rise to counter-rotating pairs of streamwise-oriented vortices known as Görtler vortices, Taylor vortices, and Dean vortices, respectively. Such vortices were first observed in the laminar flow regime, but the existence of their turbulent analogue has later been confirmed. The presence of such longitudinal vortices or roll cells gives rise to excessive cross-stream mixing and certainly affects the skin-friction drag and the heat transfer rate.

The present study is concerned with Dean flow [1], i.e. the pressure-driven flow in a curved channel bounded by two cylindrical surfaces. This flow is probably of greater engineering importance than the far more popular Taylor–Couette flow. The instability and the transition in Dean flow were investigated theoretically and numerically by Finlay *et al.* [2] and experimentally by Matsson and Alfredsson [3]. Direct numerical simulations (DNS) of turbulent curved-channel flow were first performed by Moser and Moin [4] for a weakly curved channel. They observed asymmetries in the resulting turbulence statistics and a distinct pair of counter-rotating roll cells. Such large-scale longitudinal vortices were thereafter observed experimentally by Kobayashi and Maekawa [5] using hot-wire anemometry. More recently, Nagata and Kasagi [6] performed curved-channel DNS for four different curvature ratios, whereas Xu *et al.* [7] actively controlled the Dean vortices that arose in their DNS and thereby reduced the skin friction.

In order to perform direct (or large-eddy) simulations of the turbulent flow field along a curved surface the (filtered) Navier–Stokes equations can be expressed in curvilinear or body-fitted coordinates. Taylor–Couette flow and Dean flows are more conveniently studied by using cylindrical coordinates. However, the majority of well-documented DNS and large-eddy simulation (LES) codes are available only in Cartesian coordinates. Although DNS and LES solvers in which the Navier–Stokes equations are formulated in other coordinate systems, e.g. cylindrical, spherical, and even generalized coordinates, are being used today, the post-processing of data required for structural analysis is considerably simpler in Cartesian coordinates than in any other coordinate system. The aim of the present study is therefore to derive the primary curvature corrections to the Navier–Stokes equations, which are believed to account for modest streamline curvature. First-order curvature corrections to the Navier–Stokes equations in Cartesian coordinates are rigorously derived from the full Navier–Stokes equations in cylindrical coordinates in Section 3, after first having defined the curved-channel flow problem in Section 2. The numerical approach and the computational parameters are presented in Section 4, before the results of the present approach are compared with DNS data from [4, 6] in Section 5.

2. DEAN FLOW IN CURVED-CHANNEL CONFIGURATION

We consider the pressure-driven incompressible flow of a viscous fluid in a curved channel as illustrated in Figure 1. The flow is confined between two concentric cylinders with radii of curvature R_{in} and R_{out}, respectively. The radius of curvature at the centerline is thus $R_{\text{c}} = \frac{1}{2}(R_{\text{out}} + R_{\text{in}})$ and the channel half-width $\delta = \frac{1}{2}(R_{\text{out}} - R_{\text{in}})$. The ratio δ/R_{c} is defined as the dimensionless curvature parameter. In the limiting case of infinitely large radius of curvature, δ/R_{c} goes to zero and the plane channel flow limit is obtained.

The imposed mean pressure gradient $C_p \equiv -\partial\overline{P}/\partial\theta > 0$ drives the flow in the azimuthal (θ) direction of the cylindrical coordinate system shown in Figure 1. Irrespective of whether the flow is laminar or turbulent, a mean pressure gradient $\partial\overline{P}/\partial r$ is set up in the radial (r) direction in order to balance the centrifugal force due to the streamline curvature. The mean pressure is therefore

DOI: 10.1002/fld

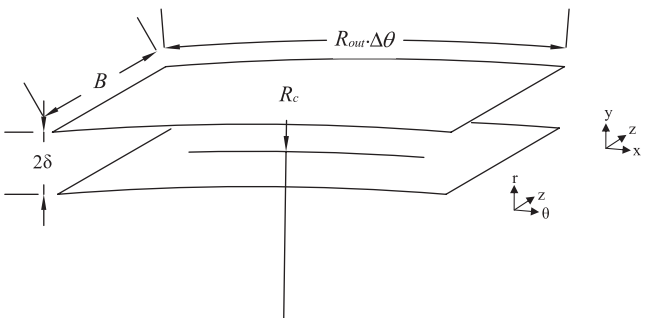

Figure 1. Curved-channel configuration and the cylindrical (r, θ, z) and Cartesian (y, x, z) coordinate systems. $R_c = \frac{1}{2}(R_{out} + R_{in})$ is the mean radius of curvature.

consistently higher along the outer surface than along the inner wall. This gives rise to the notion of pressure and suction sides for the concave and convex surfaces, respectively. Provided that the flow considered is statistically homogeneous in time and in the streamwise θ-direction, a global torque balance gives

$$\tau_{in} R_{in}^2 + \tau_{out} R_{out}^2 = C_p (R_{out}^2 - R_{in}^2)/2 \equiv 2\rho u_\tau^2 R_c^2 \tag{1}$$

Here τ_{in} and τ_{out} denote the magnitude of the mean shear stresses along the inner and outer surfaces, respectively. Equation (1) states that the torque about the center of curvature ($r = 0$) exerted by the imposed azimuthal pressure gradient is balanced by the torques associated with the skin friction along the curved walls. The corresponding balance equation (2.2) in [4] is unfortunately dimensionally inconsistent.

Owing to the asymmetry of the pressure-driven flow in a curved channel, the wall shear stresses τ_{in} and τ_{out} are generally different and the *global* friction velocity u_τ defined by Equation (1) becomes a representative measure of the overall flow resistance. The present definition of the global friction velocity is consistent with that used in [6]. Local friction velocities are, however, defined in accordance with the corresponding shear stresses $u_{\tau i}^2 \equiv \tau_{in}/\rho$ and $u_{\tau o}^2 \equiv \tau_{out}/\rho$.

3. MATHEMATICAL FORMULATION

The full Navier–Stokes equations for an incompressible fluid are first written in cylindrical coordinates (r, θ, z) in the radial, azimuthal, and axial directions. The corresponding velocity components (u_r, u_θ, u_z) are governed by the respective momentum equations:

$$\begin{aligned}
&\frac{\partial u_r}{\partial t} + (\vec{u} \cdot \vec{\nabla}) u_r - \nu \nabla^2 u_r + \frac{1}{\rho}\frac{\partial p}{\partial r} = \frac{1}{r} u_\theta^2 + \nu \left(\frac{1}{r}\frac{\partial u_r}{\partial r} - \frac{2}{r^2}\frac{\partial u_\theta}{\partial \theta} - \frac{u_r}{r^2} \right) \\
&\frac{\partial u_\theta}{\partial t} + (\vec{u} \cdot \vec{\nabla}) u_\theta - \nu \nabla^2 u_\theta + \frac{1}{\rho r}\frac{\partial p}{\partial \theta} = -\frac{1}{r} u_r u_\theta + \nu \left(\frac{1}{r}\frac{\partial u_\theta}{\partial r} + \frac{2}{r^2}\frac{\partial u_r}{\partial \theta} - \frac{u_\theta}{r^2} \right) \\
&\frac{\partial u_z}{\partial t} + (\vec{u} \cdot \vec{\nabla}) u_z - \nu \nabla^2 u_z + \frac{1}{\rho}\frac{\partial p}{\partial z} = \nu \left(\frac{1}{r}\frac{\partial u_z}{\partial r} \right)
\end{aligned} \tag{2}$$

DOI: 10.1002/fld

where ρ and ν are the density and the kinematic viscosity of the fluid. Mass conservation, i.e. continuity, is given by

$$\vec{\nabla} \cdot \vec{u} = -\frac{u_r}{r} \tag{3}$$

Here, the two differential operators $\vec{\nabla}$ and ∇^2 are defined as

$$\vec{\nabla} = e_r \frac{\partial}{\partial r} + e_\theta \frac{1}{r} \frac{\partial}{\partial \theta} + e_z \frac{\partial}{\partial z} \tag{4a}$$

$$\nabla^2 = \frac{\partial^2}{\partial r^2} + \frac{1}{r^2} \frac{\partial^2}{\partial \theta^2} + \frac{\partial^2}{\partial z^2} \tag{4b}$$

The momentum and continuity equations have purposely been arranged such that the left-hand sides correspond to the Navier–Stokes equations in a Cartesian coordinate system (y, x, z), provided that y and x are taken as r and θr, respectively. With this identification, the operators $\vec{\nabla}$ and ∇^2 become the standard gradient and Laplace operators in Cartesian coordinates.

The mathematical model given above is convenient to represent a flow that mainly is confined to (θ, z) surfaces, i.e. curved surfaces with radius of curvature r. In the curved-channel flow of particular concern herein, we assume that the radius of curvature is much larger than the wall separation 2δ (see Figure 1). This assumption implies that the radial coordinate r is approximately constant within the channel.

In order to simplify the system of governing equations, we first recast the problem into dimensionless form by introducing the representative scales u_τ, δ, δ/u_τ, and ρu_τ^2 for velocity, length, time, and pressure. To simplify the notation, the symbols for the dimensionless variables are the same as for the dimensional ones:

$$\begin{aligned}
&\frac{\partial u_r}{\partial t} + (\vec{u} \cdot \vec{\nabla}) u_r - \frac{1}{Re} \nabla^2 u_r + \frac{\partial p}{\partial r} = \frac{\delta}{R_c} \frac{u_\theta^2}{r} + \frac{1}{Re} \frac{\delta}{R_c} \left(\frac{\partial u_r}{\partial r} - \frac{2}{r} \frac{\partial u_\theta}{\partial \theta} \right) - \frac{1}{Re} \left(\frac{\delta}{R_c} \right)^2 u_r \\
&\frac{\partial u_\theta}{\partial t} + (\vec{u} \cdot \vec{\nabla}) u_\theta - \frac{1}{Re} \nabla^2 u_\theta + \frac{1}{r} \frac{\partial p}{\partial \theta} = -\frac{\delta}{R_c} \frac{u_r u_\theta}{r} + \frac{1}{Re} \frac{\delta}{R_c} \left(\frac{\partial u_\theta}{\partial r} + \frac{2}{r} \frac{\partial u_r}{\partial \theta} \right) \\
&\qquad\qquad - \frac{1}{Re} \left(\frac{\delta}{R_c} \right)^2 u_\theta \\
&\frac{\partial u_z}{\partial t} + (\vec{u} \cdot \vec{\nabla}) u_z - \frac{1}{Re} \nabla^2 u_z + \frac{\partial p}{\partial z} = \frac{1}{Re} \frac{\delta}{R_c} \frac{\partial u_z}{\partial r}
\end{aligned} \tag{5}$$

Mass conservation correspondingly becomes

$$\vec{\nabla} \cdot \vec{u} = -\frac{\delta}{R_c} u_r \tag{6}$$

Here, Re is the Reynolds number based on the scaling velocity and length u_τ and δ, i.e. $Re = u_\tau \delta / \nu$. Of particular relevance in the present study is the length scale ratio δ/R_c, i.e. the ratio between the channel half-width δ and the radius of curvature R_c. This dimensionless parameter distinguishes between *mild* curvature ($\delta/R_c \approx 0.01$) and *strong* curvature ($\delta/R_c \gg 0.01$). It is readily seen that all terms on the right-hand sides of Equations (5)–(6) vanish in the limit of vanishing curvature $\delta/R_c \to 0$, i.e. when the radius of curvature R_c becomes infinitely large.

DOI: 10.1002/fld

Let us assume that the curvature parameter δ/R_c is small so that the terms of order $(\delta/R_c)^2$ can be neglected and only first-order curvature terms are retained. If the cylindrical coordinates (r, θ, z) are recast into Cartesian coordinates (y, x, z) by means of the identifications $y = r$, $x = \theta r$, and $\partial/\partial x = R_c^{-1}\partial/\partial\theta$, we arrive at the following system:

$$\frac{\partial v}{\partial t} + (\vec{u} \cdot \vec{\nabla})v - \frac{1}{Re}\nabla^2 v + \frac{\partial p}{\partial y} = \frac{\delta}{R_c}u^2 + \frac{1}{Re}\frac{\delta}{R_c}\left(\frac{\partial v}{\partial y} - 2\frac{\partial u}{\partial x}\right) \tag{7a}$$

$$\frac{\partial u}{\partial t} + (\vec{u} \cdot \vec{\nabla})u - \frac{1}{Re}\nabla^2 u + \frac{\partial p}{\partial x} = -\frac{\delta}{R_c}uv + \frac{1}{Re}\frac{\delta}{R_c}\left(\frac{\partial u}{\partial y} + 2\frac{\partial v}{\partial x}\right) \tag{7b}$$

$$\frac{\partial w}{\partial t} + (\vec{u} \cdot \vec{\nabla})w - \frac{1}{Re}\nabla^2 w + \frac{\partial p}{\partial z} = \frac{1}{Re}\frac{\delta}{R_c}\frac{\partial w}{\partial y} \tag{7c}$$

$$\vec{\nabla} \cdot \vec{u} = -\frac{\delta}{R_c}v \tag{8}$$

Here, the velocity vector $\vec{u} = (v, u, w)$ is now referred to the Cartesian coordinates (y, x, z) where y is in the wall-normal direction, x is in the streamwise direction, and z is still in the spanwise direction (see Figure 1). It should be pointed out that both the cylindrical coordinate system (r, θ, z) and the Cartesian coordinate system (y, x, z) are right-hand systems.

The above set of equations constitutes an approximate Navier–Stokes system for weakly curved-channel flow. Terms to second order in the curvature parameter δ/R_c have been neglected both in the streamwise and wall-normal momentum equations, whereas the only approximation invoked in the spanwise momentum equation and the continuity equation is that the local radius of curvature r is replaced by the mean radius of curvature R_c. This narrow-gap approximation to the full Navier–Stokes equations is assumed to be reliable provided that $\delta/R_c \ll 1$.

4. NUMERICAL APPROACH

The first-order curvature terms on the right-hand sides of Equations (7)–(8) are believed to account for the primary effects of streamline curvature, whereas the neglected higher-order terms are supposed to be of minor importance unless strongly curved flows are considered. In order to verify this assumption, these terms were implemented in the well-documented DNS solver MGLET [8].

MGLET is a finite-volume code in which the Navier–Stokes equations are discretized on a staggered Cartesian mesh with non-equidistant grid spacing. The discretization is second-order accurate in space. For the time integration an explicit third-order Runge–Kutta scheme is used. The Poisson equation for the pressure is solved by Stone's Strongly Implicit Procedure.

Since we are concerned only with fully developed flow in a curved channel, the boundary conditions are the same as those routinely used in DNS of plane Poiseuille flow. Periodic conditions are therefore used in the homogeneous streamwise (x) and spanwise (z) directions. No-slip conditions are imposed at the solid inner and outer surfaces.

Numerical simulations were performed for two slightly different cases, with the curvature parameter $\delta/R_c = 0.0127$ (Case 1) and $\delta/R_c = 0.013$ (Case 2). This weakly curved-channel flow corresponds to the case considered by Moser and Moin [4] at $Re = 168$ and more recently by Nagata and Kasagi [6] at $Re = 150$. The modest difference in Reynolds number between the two reference

DOI: 10.1002/fld

Table I. Computational parameters for the present Cases 1 and 2 compared with the corresponding reference cases.

Simulation	Re	L_c/δ	B/δ	Δx^+	Δz^+	Δy^+_{min}	Δy^+_{max}
Moser and Moin	168	12.64	$4\pi/3$	18	6	0.2	8.2
Xu *et al.*	170	4π	$8\pi/3$	36	12	—	—
Nagata and Kasagi	150	2.5π	π	18.3	7.35	0.16	6.07
Present Case 1	168	12.64	$4\pi/3$	16.6	5.5	0.34	6.6
Present Case 2	150	2.5π	π	18.3	7.35	0.3	5.92

The length L_c of the computational domain and the streamwise grid spacing $\Delta x = R_c \Delta\theta$ are measured along the centerline in the earlier studies in which a curved domain was used.

cases is probably of minor importance than the different sizes of the computational domain used. For that reason we performed a simulation (Case 1) at $Re = 168$ with a computational domain of the same length (L) and width (B) as that used in [4], whereas the present Case 2 at $Re = 150$ was performed with the same domain as in [6]; see Table I. In addition, some results from Case 2 with moderate curvature $\delta/R_c = 0.05$ rather than weak curvature $\delta/R_c = 0.013$ will be shown.

The present simulations were carried out with $128 \times 128 \times 128$ (Case 1) and $128 \times 64 \times 64$ (Case 2) grid points in the wall-normal, streamwise, and spanwise directions, respectively. The grid points were equally distributed in the two homogeneous directions with constant grid spacing Δx^+ and Δz^+ (measured in wall units) in the streamwise and spanwise directions, respectively. A non-uniform mesh distribution was used in the wall-normal y-direction to adequately resolve the turbulence scales in the vicinity of the walls. The first grid point away from the wall was at $\Delta y^+ \approx 0.3$, whereas $\Delta y^+ \approx 6$ in the center (for details, see Table I).

The simulations were started from an instantaneous flow field from a fully developed plane channel flow simulation and thereafter let to evolve to a new statistically steady state. The same time step $\Delta t = 0.0005\delta/u_\tau$ as that used in [4] was used in both cases. Statistics were gathered for $6\delta/u_\tau$ after the flow field first had evolved into a statistically steady state.

5. RESULTS AND COMPARISONS

All results reported in this section are for weakly curved-channel flow with $\delta/R_c \approx 0.013$ and moderately curved-channel flow with $\delta/R_c \approx 0.05$. The present simplified Navier–Stokes model is believed to be accurate for the modest curvature. Nagata and Kasagi [6] also reported results for some higher curvature ratios up to $\delta/R_c = 0.20$.

5.1. Mean flow and turbulence statistics

The mean flow and turbulence statistics presented in this section are subjected to averaging in both the streamwise and spanwise directions. In Figure 2 the mean velocity for Case 1 is plotted in law-of-the-wall coordinates, where U^+ and y^+ are based on the local wall-friction velocities $u_{\tau i}$ and $u_{\tau o}$ introduced in the last paragraph of Section 2. With this scaling, the two mean velocity profiles are nearly indistinguishable in the innermost wall layer up to about $y^+ \approx 8$. Further away from the walls, the mean velocity in the inner (convex) part of the curved channel exceeds U^+ in the outer (concave) part.

DOI: 10.1002/fld

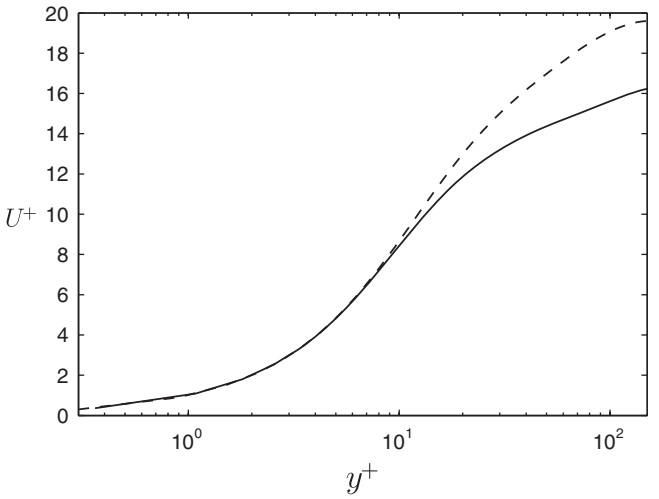

Figure 2. Mean velocity profile in local wall coordinates for Case 1. ——, concave wall; - - - -, convex wall.

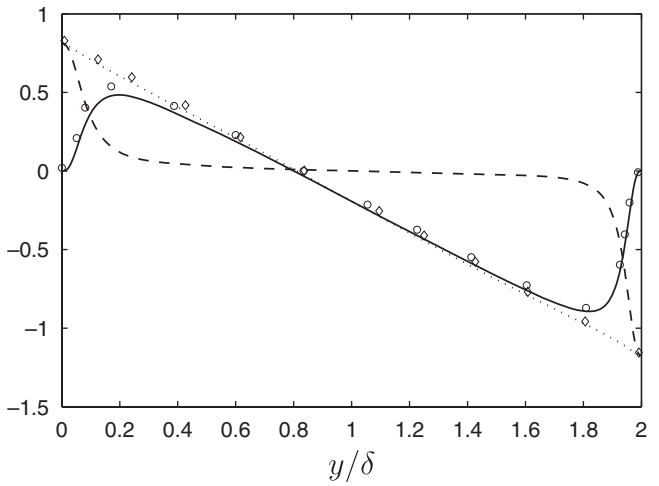

Figure 3. Shear stress variations across the curved channel for Case 1. - - - -, viscous shear stress; ——, ○, turbulent shear stress; ·····, ◇, total shear stress τ. Normalized by ρu_τ^2. The symbols denote data from [4].

The variation of the total mean shear stress

$$\tau = \mu r \frac{\mathrm{d}}{\mathrm{d}r}\left(\frac{U}{r}\right) - \rho\overline{uv} \tag{9}$$

across the curved channel is shown in Figure 3, together with its two constituents. The viscous shear stress dominates in the innermost wall regions, whereas the turbulent shear stress exceeds the

DOI: 10.1002/fld

viscous shear over 90% of the cross-section and exhibits a nearly linear variation over the middle of the channel. In a plane channel the shear stress distributions are perfectly anti-symmetric. In the present curved-channel flow, the zero-crossing is shifted toward the inner (convex) wall and the magnitude τ_{out} of the wall shear stress at the outer (concave) surface is substantially higher than the wall friction τ_{in} at the inner surface. These asymmetries are fully consistent with the observations reported in [4]. Local Reynolds numbers Re_{i} and Re_{o} based on the local friction velocities $u_{\tau\text{i}}^2 \equiv \tau_{\text{in}}/\rho$ and $u_{\tau\text{o}}^2 \equiv \tau_{\text{out}}/\rho$ are provided in Table II. A nearly perfect agreement with the data reported in [4] can be observed, while some deviations with data deduced from [6] exist. It might be useful to compare the global Reynolds number with the local Reynolds numbers at the inner and outer surfaces. The definition of the global friction velocity (1) can easily be rearranged to

$$Re_{\text{i}}^2 \left(1 - \frac{\delta}{R_{\text{c}}}\right)^2 + Re_{\text{o}}^2 \left(1 - \frac{\delta}{R_{\text{c}}}\right)^2 = 2Re^2 \tag{10}$$

The global Reynolds number Re deduced from Equation (10) has also been reported in Table II. The close correspondence between Re obtained from Equation (10) and Re associated with the imposed azimuthal pressure gradient C_p suggests that the sampling is sufficient.

The turbulent intensities (root-mean-square of the velocity fluctuations) are shown in Figure 4 for both cases. Case 1 results compare favorably with the curved-channel data in [4] for Reynolds

Table II. Results for the present Cases 1 and 2 compared with the corresponding reference cases.

Simulations	Re	Re_{i}	Re_{o}	Re from (10)
Moser and Moin	168	155	180	168.30
Nagata and Kasagi	150	128	160	145.31
Xu *et al.*	170	153	182	168.51
Present Case 1	168	150.41	180.52	166.54
Present Case 2	150	135.22	163.97	150.67

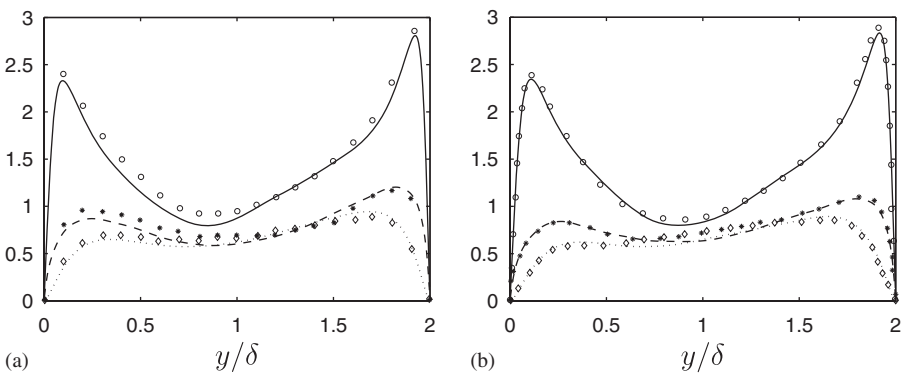

Figure 4. Turbulent intensities scaled with the global friction velocity u_τ. ——, streamwise direction; ·····, wall-normal direction; - - - -, spanwise direction. (a) Case 1 compared with data from [4]. (b) Case 2 compared with data from [6].

DOI: 10.1002/fld

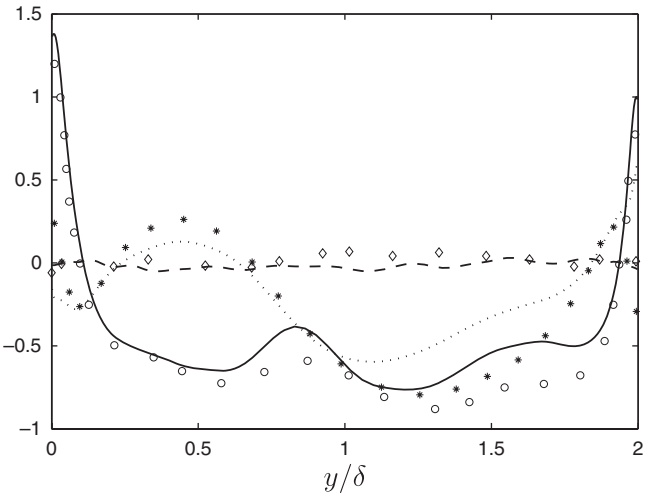

Figure 5. Skewness of the three different velocity components for Case 1. ——, streamwise direction; ·····, wall-normal direction; - - - -, spanwise direction. The symbols denote data from [4].

number $Re = 168$ in Figure 4(a), as do the Case 2 results with DNS data of [6] for $Re = 150$ in Figure 4(b). The results from both cases consistently show higher turbulence levels near the concave wall than those seen near the inner wall. These distinct asymmetries are caused by extra production terms in the transport equations for the individual Reynolds stress components, as discussed by Nagata and Kasagi [6].

Skewness factors of the velocity fluctuations are presented in Figure 5 for Case 1. The skewness of the spanwise velocity component $S(w)$ is practically zero and this supports the adequacy of the sampling time. $S(u)$ exhibits the same asymmetric behavior as already observed in [4] with the most noticeable feature being the substantially higher wall value at the convex side than at the concave wall. Also $S(v)$ shows the same qualitative behavior as the Moser and Moin [4] data in the inner part of channel cross-section. However, the present $S(v)$ reaches a maximum value at the convex wall, whereas the data in [4] exhibit a local peak at about 15 wall units away from the outer surface.

5.2. *Results with moderately strong curvature* $\delta/R_c = 0.05$

Moser and Moin [4] simulated only the weakly curved channel corresponding to the present Case 1, whereas Nagata and Kasagi [6] in their more recent investigation considered a range of curvature ratios from 0.013 (the present Case 2) to 0.20. With the view to examine how well the 'narrow-gap' approximation reproduces the curvature effects in a moderately curved channel, Case 2 was reconsidered with the curvature parameter $\delta/R_c = 0.05$. The mean velocity profile and the turbulence intensities presented in Figure 6 compare surprisingly well with the DNS data of Nagata and Kasagi [6], especially near the outer (concave) wall. The turbulence has been substantially damped along the inner (convex) wall and correspondingly enhanced near the outer surface due to the streamline curvature. The asymmetries are by far more distinct than for Case 1 with mild curvature (see Figure 4(b)).

DOI: 10.1002/fld

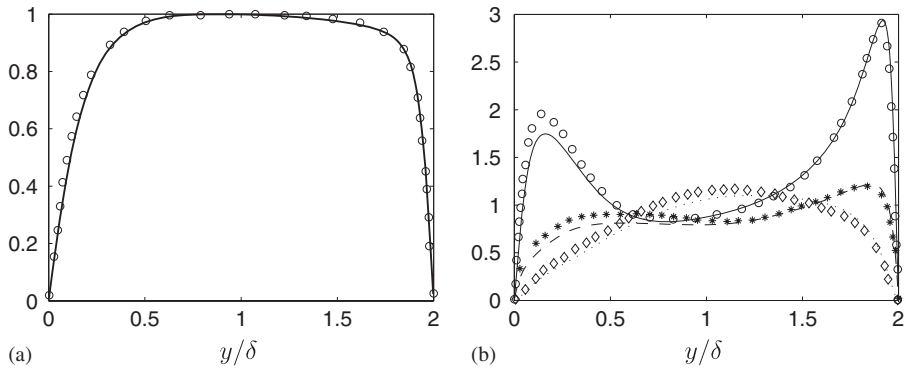

Figure 6. Case 2 but with $\delta/R_c = 0.05$. (a) Mean velocity profile scaled with the maximum mean velocity. (b) Turbulent intensities scaled with the global friction velocity u_τ: ——, streamwise direction; ·····, wall-normal direction; - - - -, spanwise direction. The symbols denote data from [6].

It should be recalled that only terms of the order $(\delta/R_c)^2$ were neglected in the 'narrow-gap' approximation, which led to the present set of simplified governing equations (7)–(8), whereas terms of the order δ/R_c were retained. Accordingly, DNS using the 'narrow-gap' approximation should be expected to provide realistic results if δ/R_c is of the order 0.01, while the predictions can be expected to gradually deteriorate when δ/R_c becomes of the order 0.1.

5.3. Dean vortices

Owing to a centrifugal instability mechanism, flows exhibiting curved streamlines may develop secondary motions perpendicular to the primary flow. Pairs of counter-rotating vortices are a commonly observed feature both in Taylor–Couette flow and boundary layer flow along a concave surface. Such roll cells may also develop in curved-channel flow (Dean flow) and are accordingly known as Dean vortices; see e.g. [2, 3]. The Dean vortices arise from the same instability mechanism as the secondary roll cells developing in other flows with streamline curvature. For this reason roll cells in curved-channel flow are sometimes called Taylor–Görtler vortices, e.g. [4, 5, 7].

In order to see whether or not Dean vortices are embedded in the present flow field, the instantaneous velocity field was averaged only in the streamwise direction x and in time t. The averaged field then becomes a function of the cross-sectional coordinates y and z and thus contains information about the Dean vortices, if any. By subtracting the conventionally averaged flow field (averaged in x, z, and t), we are left with the secondary flow field. The streamlines of this secondary flow are shown in Figure 7(a) for Case 1 and in Figure 7(b) for Case 2. In both cases one pair of counter-rotating roll cells can be observed, i.e. a roll-cell pair fills the width of the computational domain. Moser and Moin [4] pointed out that the periodic boundary conditions used in the spanwise direction have the effect of restricting the possible wavelengths of the Dean vortices. The wavelength in the present Case 1 is the same as that found by Moser and Moin [4], whereas the wavelength in the present Case 2 is slightly smaller. This is more likely due to the narrower computational domain than to the somewhat lower Reynolds number. Nagata and Kasagi [6] did not report on Dean cells from their simulations, whereas Kobayashi and Maekawa [5] observed

DOI: 10.1002/fld

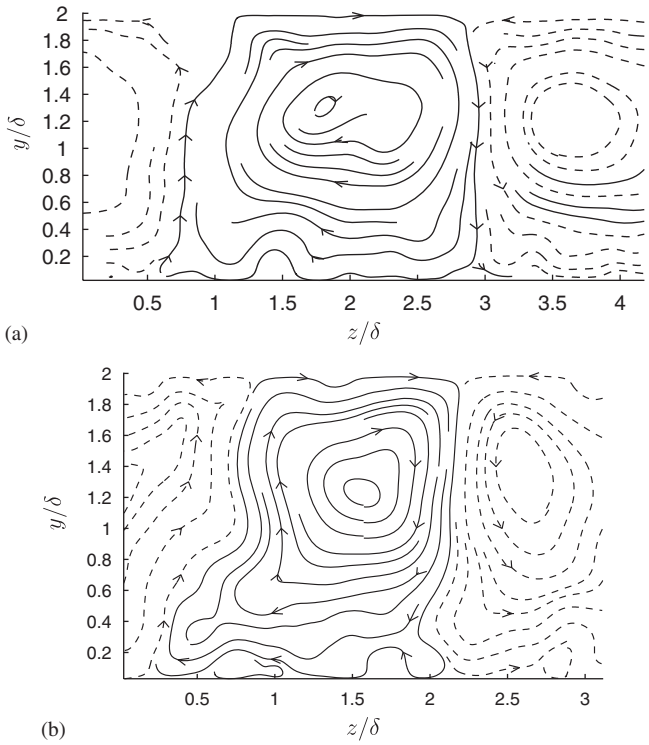

Figure 7. Dean vortices in weakly curved-channel flow: (a) Case 1 $Re = 168$ and (b) Case 2 $Re = 150$.

distinct vortex pairs in their laboratory experiments. Xu *et al.* [7] recently proposed an active controlling scheme and succeeded to attenuate the Dean vortices in their DNS study.

6. CONCLUDING REMARKS

A set of momentum equations valid for flows with weak streamline curvature has been derived from the full Navier–Stokes equations in cylindrical coordinates. Terms to first order in the curvature parameter δ/R_c were derived and implemented in a Navier–Stokes solver using Cartesian coordinates. Results from DNS achieved by integrating the simplified Navier–Stokes model for $\delta/R_c \approx 0.013$ were compared with DNS data [4, 6] acquired by integration of the full equations. The curvature-induced alterations of the mean velocity profile and the asymmetries in the Reynolds stress profiles are excellently reproduced by the present narrow-gap approach. Even for $\delta/R_c = 0.05$ reasonably good correspondence with earlier DNS data [6] was observed. The underlying mechanism responsible for the development of counter-rotating longitudinal Dean vortices is retained in the simplified model.

The simplified Navier–Stokes equations derived in the present paper are believed to perform equally well for other flows with moderate streamline curvature. Mildly curved turbulent boundary layers (Görtler flow) and narrow-gap turbulent Taylor–Couette flow can thus be simulated with

DOI: 10.1002/fld

DNS or LES codes in Cartesian coordinates provided that the first-order curvature correction terms are implemented in the flow solver.

ACKNOWLEDGEMENTS

Computer time was granted by The Research Council of Norway (Programme for Supercomputing) and NTNU (Research Programme for Computational Science and Visualization).

REFERENCES

1. Dean WR. Fluid motion in a curved channel. *Proceedings of the Royal Society of London A* 1928; **121**:402–420.
2. Finlay WH, Keller JB, Ferziger JH. Instability and transition in curved channel flow. *Journal of Fluid Mechanics* 1988; **194**:417–456.
3. Matsson OJE, Alfredsson PH. Experiments on instabilities in curved channel flow. *Physics of Fluids A* 1992; **4**:1666–1676.
4. Moser RD, Moin P. The effects of curvature in wall-bounded turbulent flows. *Journal of Fluid Mechanics* 1987; **175**:479–510.
5. Kobayashi M, Maekawa H. Turbulent flow accompanied by Taylor–Görtler vortices in a two-dimensional curved channel. *Flow Measurement and Instrumentation* 1995; **6**:93–100.
6. Nagata M, Kasagi N. Spatio-temporal evolution of coherent vortices in wall turbulence with streamwise curvature. *Journal of Turbulence* 2004; **5**:017.
7. Xu C-X, Choi J-I, Sung HJ. Identification and control of Taylor–Görtler vortices in turbulent curved channel flow. *AIAA Journal* 2003; **41**:2387–2393.
8. Manhart M. A zonal algorithm for DNS of turbulent boundary layers. *Computers and Fluids* 2004; **33**:435–461.

DOI: 10.1002/fld